Modeling of diatomic predissociation resonances within the Optimizer project

Vladimir B. Sovkov [a,b,*], Jizhou Wu [a,c], Jie Ma [a,c], Feng Xie [d], A.M. Lyyra [e], Ergin Ahmed [e]

[a] *State Key Laboratory of Quantum Optics and Quantum Optics Devices, Institute of Laser Spectroscopy, College of Physics and Electronics, Shanxi University, Taiyuan 030006, China*

[b] *St. Petersburg State University, 7/9 Universitetskaya nab., St. Petersburg 199034, Russia*

[c] *Collaborative Innovation Center of Extreme Optics, Shanxi University, Taiyuan, Shanxi 030006, China*

[d] *Institute of Nuclear and New Energy Technology, Collaborative Innovation Center of Advanced Nuclear Energy Technology, Key Laboratory of Advanced Reactor Engineering and Safety of Ministry of Education, Tsinghua University, Beijing 100084, China*

[e] *Physics Department, Temple University, Philadelphia, PA 19122, USA*

A B S T R A C T

The simulation of the predissociation spectrum of the Na_2 $2^3\Pi_g \sim 3^3\Pi_g \leftarrow b^3\Pi_u$ ($v = 14$, $J = 14$) transition, observed earlier with the Perturbation Facilitated Optical–Optical Double Resonance (PFOODR) experimental method, is done within the Optimizer project with our Split-operator computational package using Padé approximations for all functions involved in the model. This simulation reproduces the experimental spectrum satisfactory well. The parameters of the model functions involved in the simulations are determined and reported. A brief description of our computational methods and programs is presented.

Introduction

We have developed the Optimizer project [1,2] in various versions over time during the last three decades or more. Although we believe that its main application is the analysis of molecular spectra it can also be used more broadly including problems that require optimization in various fields of science such as engineering and technology, for example. Most of our scientific results (*e.g.*, [3–19] and references therein) were possible by using the Optimizer project.

The Optimizer project facilitates construction and optimization of complicated mathematical models of a versatile nature. The optimization process relies on using the familiar Levenberg–Marquardt algorithm [20,21] based on Singular Value Decomposition (SVD) [22] of the design matrix, which when needed, can be switched to any other one. It supports various methods of problem regularization, robust estimators and tools to parallelize the computation, for example.

The model construction can be done block-by-block from relatively simple "standard" modeling programs (blocks) with a convenient universal mechanism of transferring data from block to block. The program codes are subjected to some conventional regulations enabling them to be easily embedded into the entire Optimizer model. A library of such modeling programs is available for general approximation problems in addition to computational molecular spectroscopy along with the main Optimizer package, which is continually improved and extended.

All program components are written in MATLAB algorithmic language and can be executed using the MATLAB [23] or OCTAVE [24] environments. They are available with detailed instruction manuals and test samples for a free download [2] on the Internet.

The predissociation spectrum of the Na_2 $2^3\Pi_g \sim 3^3\Pi_g \leftarrow b^3\Pi_u$ ($v = 14$, $J = 14$) transition was observed and reported by Liu et al. in [25]. The experimental technique was based on the Perturbation Facilitated Optical–Optical Double Resonance (PFOODR) technique [3,7,26–36] to probe excited triplet states and detect fluorescence to the lower lying electronic states. The general scheme of the PFOODR experiment
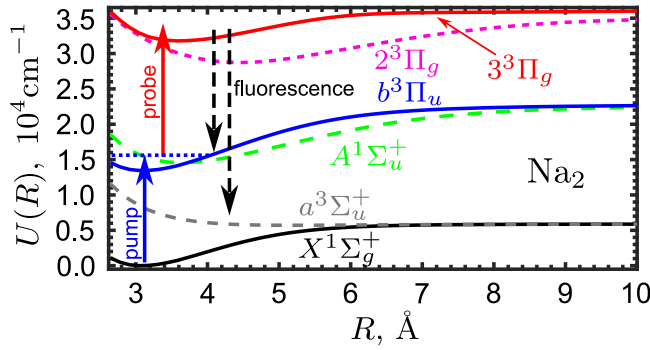
Fig. 1. (Color online) The scheme of the PFOODR experiment [25]. The pump laser excites directly the intermediate "window" level, whose approximate position is shown with the horizontal dotted line, and the probe laser excites the states of the mixed $2^3\Pi_g \sim 3^3\Pi_g$ complex above the dissociation limit of $2^3\Pi_g$ and below the one of $3^3\Pi_g$.

Ref. [25] is shown in Fig. 1 with the *ab initio* adiabatic potential energy functions of Ref. [37].

The spectrum in Fig. 2 is characterized by broad fluorescence spectral features caused by the non-adiabatic interaction between the $3^3\Pi_g$ and $2^3\Pi_g$ states as well as by additional narrower spectral lines attributed to the participation of the $4^3\Sigma_g^+$ and $2^3\Delta_g$ states. Predissociation is an example of quantum resonances, which are among the most important and intriguing phenomena in quantum physics [38,39]. During predissociation a molecule in a bound rovibrational level below the dissociation limit of its electronic state can dissociate into atoms by coupling to a continuum level that belongs to a lower lying electronic state above its dissociation limit. Inverse predissociation can also play a role in the formation of molecules in the interstellar molecular clouds, for example (see Refs. [40,41]).

A preliminary simulation (with a participation of some of us) of the predissociation spectrum of the Na$_2$ $2^3\Pi_g \sim 3^3\Pi_g \leftarrow b^3\Pi_u$ ($v = 14$, $J = 14$) transition by using the multichannel Split-Operator method [42–48] was shown at the conference [49]. A few years later Narevicius et al. [50] reported a simulation of this spectrum using the complex scaling method [51] with *ab initio* potential functions [37]. The spectrum was not reproduced quantitatively by shifting the *ab initio* potentials of the $2^3\Pi_g$ and $3^3\Pi_g$ states relative to each to optimize the widths of the resonance peaks in the simulation compared to the experiment. To the best of our knowledge, no other attempts to simulate or analyze this spectrum have been performed since then.

In the present work we have improved our multichannel Split-operator computer program and adapted it to meet the requirements of the Optimizer project. We checked its ability to simulate predissociation resonances in the predissociation spectrum being discussed in this work. For this purpose, we constructed the model of the two-channel coupling of the $3^3\Pi_g$ and $2^3\Pi_g$ states using Padé approximations [52–65] for all the functions involved. We optimized the parameters of the model to get the best reproduction of the experimental spectrum.

In the Appendix we present brief description of our computational methods and programs.

Theory and algorithms

In the diabatic representation [66], the two-channel potential is a matrix

$$U_{\text{diab}}(R) = \begin{bmatrix} V_1(R) & W(R) \\ W(R) & V_2(R) \end{bmatrix}, \tag{1}$$

where R is the interatomic distance, $V_1(R)$ and $V_2(R)$ are the diabatic potential functions of the molecular electronic states, $W(R)$ is the interaction matrix element. The eigenvalues of this matrix are the adiabatic potential functions $U_1(R)$ and $U_2(R)$ (deffer by the "+ " and "−" signs below):

$$U_{1,2}(R) = \frac{1}{2}\left[V_1(R) + V_2(R) \pm \right.$$
$$\left. \sqrt{\left(V_1(R) - V_2(R)\right)^2 + 4W^2(R)} \right], \tag{2}$$

$$V_{1,2}(R) = \frac{1}{2}\left[U_1(R) + U_2(R) \pm \right.$$
$$\left. \epsilon\sqrt{\left(U_1(R) - U_2(R)\right)^2 - 4W^2(R)} \right] \tag{3}$$

(ϵ is a conventional sign factor, which should be inverted at cross points), while the normalized eigenvectors being arranged column-wise comprise the transformation matrix from the adiabatic to the diabatic representation:

$$F_{a\to d}(R) = \begin{bmatrix} f_1^{(1)}(R) & f_2^{(1)}(R) \\ f_1^{(2)}(R) & f_2^{(2)}(R) \end{bmatrix} \tag{4}$$

with

$$\begin{cases} f_{1,2}^{(1)}(R) = t_{1,2}(R)f_{1,2}^{(2)}(R), \\ f_{1,2}^{(2)}(R) = \left(t_{1,2}^2 + 1\right)^{-1/2}, \\ t_{1,2}(R) = \left[\delta V(R) \mp \sqrt{\delta V^2(R) + 1}\right]^{-1}, \\ \delta V(R) = \dfrac{V_2(R) - V_1(R)}{2W(R)}. \end{cases} \tag{5}$$

As is well known [67], the diabatic potential functions can cross each other, while the adiabatic ones cannot and instead give rise to avoided crossing.

There are number of ambiguities in the above set of equations that need to be addressed before they can be used for specific calculations. First, the columns in Eq. (4) can be swapped, resulting in a switch of the order of the adiabatic potential functions. We choose to assign the first column of the matrix to the state with lower adiabatic potential. Second, the sign of every column of (4) is undefined, reflecting the well known arbitrariness of eigenvector phases and resulting in the change of sign of the function being transformed with the help of this matrix. The signs of the interaction function $W(R)$ relative to the signs of the transition moment functions $M_1(R)$ and $M_2(R)$ in either diabatic or adiabatic representation reflects the choice of the signs of the electronic eigenfunctions in the same representation, while a switch of a sign of a column in (4) implies a switch of the sign of a (transformed) electronic eigenfunction in one of these representations. In principle, with any consistent choice of signs at every point R independently the theory remains correct, however, it is evident that smooth functions are easier to interpret and compute. We adopted the rule that the signs of the diagonal elements $f_1^{(1)}(R)$ and $f_2^{(2)}(R)$ to coincide with the sign of $W(R)$; notice, that our final $W(R)$ occurred negative in the entire range, causing no problems with the switch of all relevant signs at a point of $W(R) = 0$.

Our computations were performed in the following way. First, we linearly transformed (warped) the *ab initio* adiabatic potentials [37] of the $3^3\Pi_g$ and $2^3\Pi_g$ states placing the long-range limit to the approximate atomic $3s + 3d$ and $3s + 4p$ energies [68] (neglecting the fine and hyperfine splitting), and the bottom at the approximate experimental energy of the potential minimum [69]. We deperturbed these potentials using Eq. (3) with the implied cross point at $R_c \approx 2.8$ Å and the constant value for $W(R) = -153$ cm^{-1} (following the rough model of [49]). Then, we fitted the diabatic potential energy curves to the Padé functions and used them as the zeroth order approximations. In contrast, the zeroth order approximations for the interaction $W(R)$ and the transition moment functions $M_1(R)$ and $M_2(R)$ were just constants.

To generate the initial wavepacket, we computed the wavefunction of the Na$_2$ $b^3\Pi_u$ ($v = 14$, $J = 14$) level with our programs of the
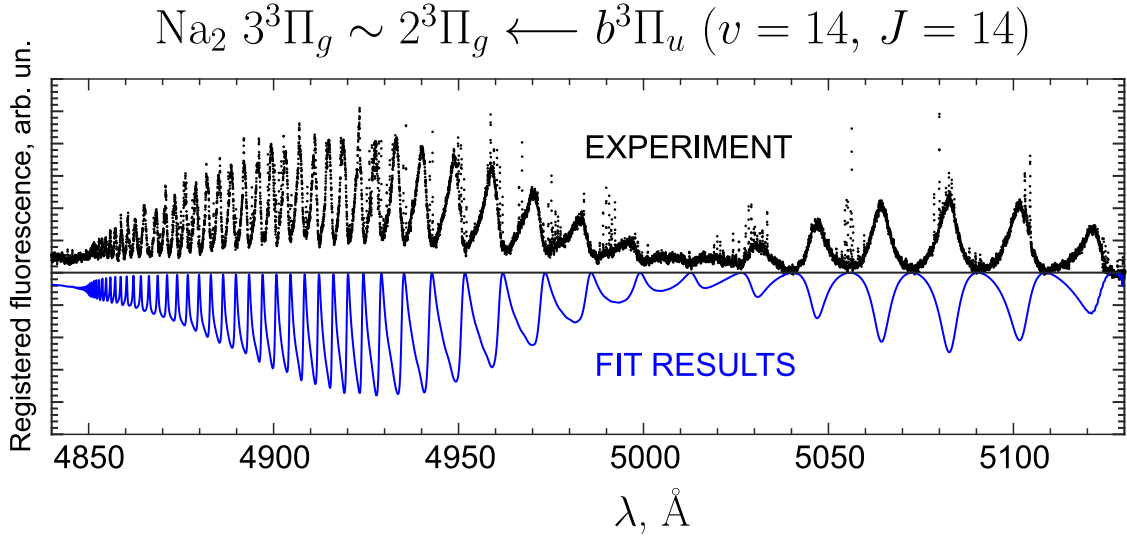
Fig. 2. (Color online) The experimental [25] and fitted predissociation spectra of the Na$_2$ $3^3\Pi_g \sim 2^3\Pi_g \longleftarrow b^3\Pi_u$ ($v = 14$, $J = 14$) transition.

Numerov method [70], already included into the Optimizer project [2]. For the potential function of the $b^3\Pi_u$ state we took the one reported in [71]. In the course of the computations we eliminated a misprint in the table II of [71]: the decimal order of the parameter a_5 of the $b^3\Pi_u$ state must be "4" in place of the reported value "5"; otherwise it was impossible to reproduce the ro-vibrational term values with this potential.

After that, the following iteratively repeated procedure was applied:

1. The diabatic potential energy functions of both states, the interaction function, and the transition moment functions were computed from their current Padé parameters at the required spatial grid points.
2. The two-channel diabatic initial wavepacket was formed by multiplying the $b^3\Pi_u$ ($v = 14$, $J = 14$) wavefunction by the transition moment functions of the corresponding channels.
3. The adiabatic potential functions were computed from the diabatic ones using Eq. (2), and the set of transformation matrices was computed using Eqs. (4) and (5).
4. Next, the two-channel evolution (the time autocorrelator) of the wavepacket in the field of the $3^3\Pi_g \sim 2^3\Pi_g$ electronic state complex was computed with our Split-operator programs.
5. The predissociation spectrum was computed using a Fourier transform of the time autocorrelator and compared with the experimental one.

Besides that, we added to the data being fitted and simulated the *ab initio* calculated [37] adiabatic potential functions and the adiabatic transition moment functions, although with rather smaller weights. Then, model parameters were corrected and the procedure was repeated until a satisfactory reproduction of the experimental spectrum was achieved.

In most computations, the spatial grid was set between 2 Å and 26.564 Å with step 0.012 Å, and the time grid spanned the 0 to 30 fs range with step of 0.001 fs (permitting computation of the time autocorrelator in the range from −60 fs to 60 fs [46]). In the long-range region, the wavepacket was damped by the cosine-type absorbing function described in our work [72] with the recommended parameters (in the designations of [72]) $E_0 = 100$ cm^{-1}, $k = 3$, $l = 4$, $\alpha = 0.266$, $l_+ = 1$, $\gamma = 1$, with its right boundary located at the very end of the spatial grid and the corresponding left boundary at $R_b = 22.76$ Å. When the main computation was finished, we tried altered parameters: reduced spatial and time steps twice, extended the time grid to 50 fs, set the reference energy of the absorbing function to $E_0 = 30$ cm^{-1},

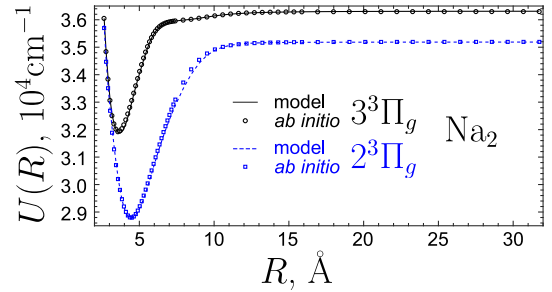**Fig. 3.** (Color online) The *ab initio* and the final model adiabatic potential energy curves of the Na$_2$ $3^3\Pi_g$ and $2^3\Pi_g$ states. The origin of the energy scale is at the bottom of the ground state Na$_2$ $X^1\Sigma_g^+$.

extended the absorbing region to $l = 6$ with $\alpha = 0.306$ [72],—and observed no noticeable change in the computed spectrum.

Results

The final simulation of the Na$_2$ $3^3\Pi_g \sim 2^3\Pi_g \longleftarrow b^3\Pi_u$ ($v = 14$, $J = 14$) predissociation spectrum is compared with the experimental one in Fig. 2.

The final Padé approximant parameters of all diabatic functions that were used to reproduce the results of the present paper, are reported in Tables 1 and 2. We would like to emphasize that the simulated spectrum in Fig. 2 was computed with the parameters in Tables 1 and 2 exactly, *i. e.* being already rounded.

The general view of the final adiabatic $3^3\Pi_g$ and $2^3\Pi_g$ state potential functions along with the *ab initio* ones is shown in Fig. 3, and a magnified view of the region of the (avoided) crossings is shown in Fig. 4.

The function of the interaction matrix element is shown in Fig. 5

The transition moment functions of the Na$_2$ $3^3\Pi_g \leftarrow b^3\Pi_u$ and $2^3\Pi_g \leftarrow b^3\Pi_u$ optical transitions in both diabatic and adiabatic representations are shown in Fig. 6 along with the *ab initio* [37] ones.

Discussion

In our opinion, the reproduction of the experimental spectrum with our final simulation in Fig. 2 is exceptionally good, with the quality

Table 1

Parameters of the Padé functions approximating the Na$_2$ $3^3\Pi_g$ and $2^3\Pi_g$ diabatic potentials involved in the model. All values are measured in Å and cm^{-1}. The origin of the energy scale is at the bottom of the ground state Na$_2$ $X^1\Sigma_g^+$. Uncertainties of the fitted model parameters are of the order of magnitude of the last decimal digit reported.

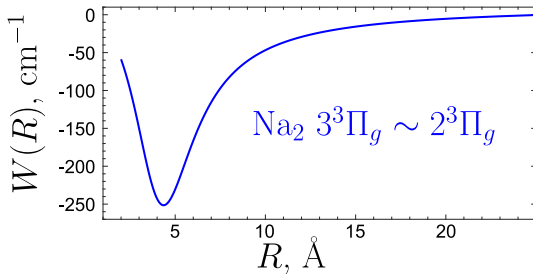| $3^3\Pi_g$				$2^3\Pi_g$			
Parameter	Value	Parameter	Value	Parameter	Value	Parameter	Value
x_0	3.686	b_0	1	x_0	4.441	b_0	1
C	36 311.4	b_1	0	C	35 188.6	b_1	0
		b_2	2840			b_2	0.97
a_0	−4467	b_3	1285	a_0	−6400	b_3	0.3
a_1	0	b_4	220	a_1	0	b_4	0.152
a_2	−1.2685e+07	b_5	330	a_2	−4800	b_5	0.045
a_3	−5.62e+06	b_6	130	a_3	−2800	b_6	−0.011
a_4	5.25e+06	b_7	−300	a_4	660	b_7	−0.0011
a_5	400 000	b_8	−27	a_5	−45	b_8	0.0009
a_6	−90 000	b_9	99				
a_7	−8.167e+05	b_{10}	29.02				
a_8	1.235e+05	b_{11}	−3.5				
a_9	15 000	b_{12}	−2.21				
a_{10}	−3450	b_{13}	0.332				
a_{11}	−1200	b_{14}	0.021				

Table 2

Parameters of the Padé functions approximating the Na$_2$ $2^3\Pi_g \sim 3^3\Pi_g$ interaction matrix element W and $3^3\Pi_g \leftarrow b^3\Pi_u$, $2^3\Pi_g \leftarrow b^3\Pi_u$ transition moments M involved in the model. All values are measured in Å, cm^{-1}, and D. Uncertainties of the fitted model parameters are of the order of magnitude of the last decimal digit reported.

$2^3\Pi_g \sim 3^3\Pi_g$, W		$3^3\Pi_g \leftarrow b^3\Pi_u$, M		$2^3\Pi_g \leftarrow b^3\Pi_u$, M	
Parameter	Value	Parameter	Value	Parameter	Value
x_0	2.906	x_0	5	x_0	5
C	0	C	0	C	5
a_0	−140	a_0	0.48	a_0	−16.3
a_1	−530	a_1	−0.55	a_1	−9
a_2	2.6	a_2	−0.4	a_2	−2.16
b_0	1	b_0	1	b_0	1
b_1	−0.4	b_1	0.9	b_1	0.49
b_2	0.2	b_2	0.2143	b_2	0.2
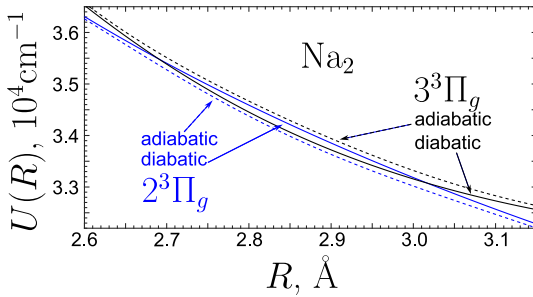
Fig. 4. (Color online) The final model diabatic (solid lines) and adiabatic (dashed lines) potential energy curves of the Na$_2$ $3^3\Pi_g$ and $2^3\Pi_g$ states in the region of the (avoided) crossings. The origin of the energy scale is at the bottom of the ground state Na$_2$ $X^1\Sigma_g^+$.

Fig. 5. (Color online) The final model interaction matrix element of the Na$_2$ $3^3\Pi_g \sim 2^3\Pi_g$ state complex.
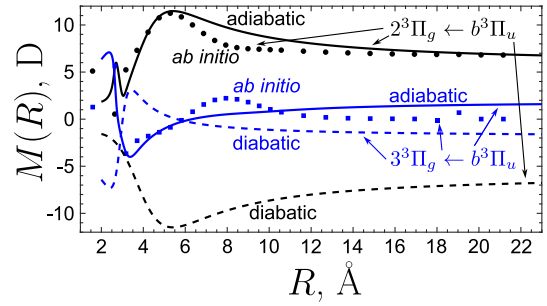
Fig. 6. (Color online) The moment functions of the Na$_2$ $3^3\Pi_g \leftarrow b^3\Pi_u$ and $2^3\Pi_g \leftarrow b^3\Pi_u$ optical transitions: dots—*ab initio*, solid lines—model adiabatic, dashed lines—model diabatic.

close to the accuracy of the experimental measurements. The wavelengths, widths, and intensities of the resonance peaks are accurately reproduced. The remaining discrepancies in the forms of some of the line profiles can be attributed to both experimental inaccuracies and restrictions of our model, including ignoring the triplet character of the states, spin–orbit mixing of the initial $b^3\Pi_u$ state with the $A^1\Sigma_u^+$ state, and perturbations from other near-lying states.

The most important factor determining the quality of this reproduction is the outer branch of the $3^3\Pi_g$ state potential above the $3s + 3d$ (lower) dissociation limit, which can be considered the most reliable quantitative result of our investigation. Other parameters are less influential but necessary for the model.

It is interesting and rather unexpected that our final potential functions have two crossing points at about 2.69 Å and 3.01 Å—see Fig. 4. The previous simulations [49,50] implied the existence of only one crossing point. It was noted [25,50] that the position of the crossing point influences the widths of the resonance peaks. Probably, ignoring the possible existence of an additional crossing point can explain the difficulty in the simulation of the spectral line widths in [50].

Our final transition moment functions in Fig. 6 are relatively close to the *ab initio* ones, however, we must recognize that the deviations remain significant, especially in the short-range region, which is the most important in the formation of the initial wavepacket.

The number of parameters of the $3^3\Pi_g$ state potential in Table 1 exceeds the analogous number of parameters of the $2^3\Pi_g$ state potential. In the beginning we tried to describe it with the same number of parameters as $2^3\Pi_g$ but were unsuccessful. Fig. 7 provides the explanation. The initial version of the function (smaller set of parameters) was unable to reproduce the bend at around 8 Å, which is clearly seen in the *ab initio* potential energy curve (Fig. 7(a)), causing significant shifts
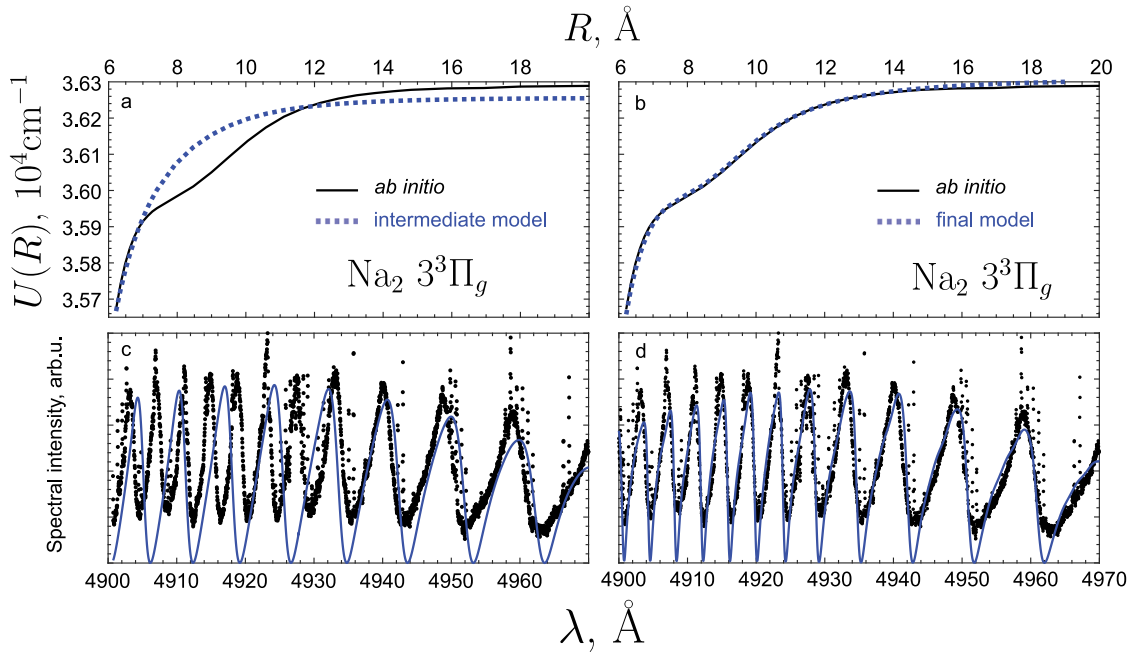
Fig. 7. (Color online) Influence of the Na$_2$ $3^3\Pi_g$ potential function bends on the predissociation spectrum: (a) adiabatic *ab initio* and intermediate model potentials; (b) adiabatic *ab initio* and final model potentials; (c) experimental (dots) and intermediate model (line) spectra; (d) experimental [25] (dots) and final model (line) spectra.

of the computed peaks in the range of wavelengths shorter than 4935 Å (Fig. 7(c)). The final version of the function (bigger set of parameters) reproduced this bend (Fig. 7(b)) and improved the positions of the computed peaks (Fig. 7(d)). On the one hand, this confirms once more the importance of even subtle features of the $3^3\Pi_g$ state potential in our model, and on the other hand, this confirms the quality of the long-range *ab initio* potentials [37], exhibiting those subtle features.

We also explored the ability of the Fourier grid method (see [73–76]) in our realization of it for the Optimizer project (see the brief description in [72] with more detail given in the manual in [2]) to predict properties of the predissociation resonances in terms of the complex energies. For this purpose, we took our final potential energy functions of the $3^3\Pi_g$ and $2^3\Pi_g$ states and the interaction function $W(R)$, and embedded the optical potential with the same parameters as of the absorbing function used in the main computation above. Embedding an optical potential makes the Fourier-grid Hamiltonian complex-type with complex-type eigenenergies. The inverse of the imaginary part of this eigenenergy is proportional to the lifetime of the decaying state, located at the energy equal to the real part of it. In Fig. 8, circles connected with the solid line (red in the online color version) are those "lifetimes" versus the real-type energies of the states.

Although some weak peaks are observed near the positions of resonances, they are not much stronger than the neighboring "non-resonant" peaks. Besides, some artifacts (deep dips) are observed, which can confuse the interpretation of the results. We suppose that the long lifetimes of the non-resonant states are caused by a long distance of the region before the absorbing function, so that the non-resonant parts of the wavepacket indeed lives there for a relatively long time. To check this, we shifted the left boundary of the absorbing region from $R_b = 22.76$ Å to $R_b = 10$ Å and repeated the computation. The result is shown in Fig. 8 as diamonds connected by the dashed line (blue in the online color version). This indeed made the resonance peaks much more prominent. This allowed us to separate the most intense peaks (biggest lifetimes) and plot them in Fig. 9 on the same scale as the experimental spectrum. Although some correspondence between the observed and calculated resonances takes place, the positions of the computed ones are noticeably shifted in the short-wavelength region.

For a comparison, we computed the unperturbed eigenenergies of the $3^3\Pi_g$ state in the diabatic representation with the Numerov method, and showed them in Figs. 8 and 9 as squares located at the abscissa. It is seen, that the positions of the model complex-type-energy resonances are closer to the experimental peaks in the long-wavelength region but deviate in the short-wavelength region, while the unperturbed eigenenergies are closer to the experimental peaks in the short-wavelength region, but deviate in the long-wavelength region. This can be explained by the fact that at the higher energies the perturbation of the $3^3\Pi_g$ states becomes weaker (in part, that is reflected by the narrower peaks), while the influence of the absorbing optical potential distorts more strongly the Fourier-grid Hamiltonian.

Overall, the approach based on the complex-type eigenenergies of the Fourier-grid Hamiltonian with the embedded optical potential seems not to be very reliable even if it can show some characteristics of the resonances. Its results strongly depend on the parameters of the optical potential and other technical details. We expect that more sophisticated methods that use the complex-type eigenenergies, such as the method of the complex scaling [50,51], are able to give much better results. However, these method are not included in the Optimizer project yet and are currently outside of the scope of our research.

The only works investigating the lower-lying bound levels of the sodium dimer states under consideration, which we are aware of, are Refs. [28,69,77,78]. However, we have not found estimates of the parameters of the interaction between the Na$_2$ $2^3\Pi_g$ and $3^3\Pi_g$ states in them, which could be compared to our results.

Conclusions

We have demonstrated the efficiency of the multichannel Split-operator method programs, embedded into the Optimizer project for description of resonance phenomena, such as molecular predissociation spectra. The experimental Na$_2$ $2^3\Pi_g \sim 3^3\Pi_g \leftarrow b^3\Pi_u$ ($v = 14$, $J = 14$) spectrum was simulated with an accuracy close to the experimental results. We also demonstrated the ability of the Padé approximants to describe all important features of the potential energy and other functions involved in the model, including subtle bends. The fitted parameters that enabled the reproduction of the results of the present
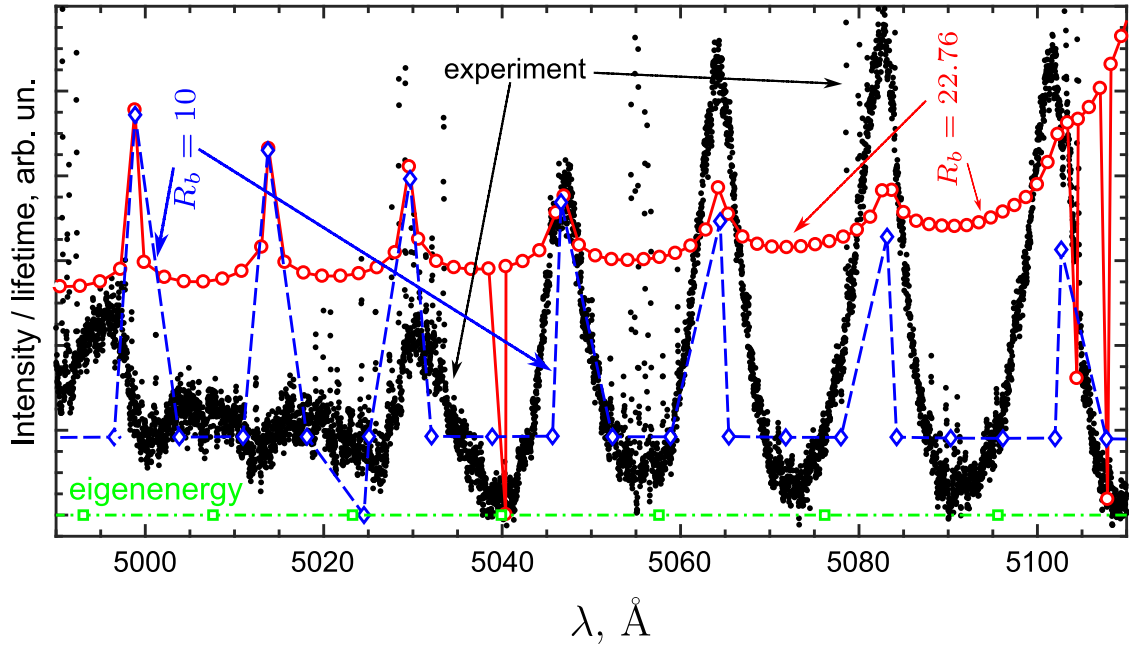
Fig. 8. The experimental [25] Na$_2$ $3^3\Pi_g \sim 2^3\Pi_g \leftarrow b^3\Pi_u$ ($v = 14$, $J = 14$) predissociation spectrum (dots), lifetimes estimated with the Fourier grid method with the optical potential starting at $R_b = 22.76$ Å (circles connected with a solid line) and $R_b = 10$ Å (diamonds connected with a dashed line), and the eigenenergies of the Na$_2$ $3^3\Pi_g$ ($J = 14$) state (squares at the abscissa). (For interpretation of the references to color in this figure legend, the reader is referred to the web version of this article.)
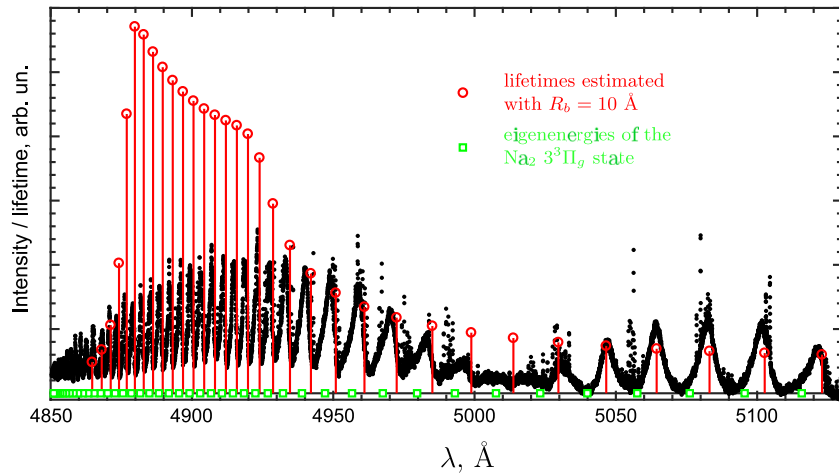
Fig. 9. (Color online) The experimental [25] Na$_2$ $3^3\Pi_g \sim 2^3\Pi_g \leftarrow b^3\Pi_u$ ($v = 14$, $J = 14$) predissociation spectrum (dots), lifetimes estimated with the Fourier grid method with the optical potential starting at $R_b = 10$ Å (circles with stems), and the eigenenergies of the Na$_2$ $3^3\Pi_g$ ($J = 14$) state (squares at the abscissa).

paper, are reported. We also showed that the straightforward computation of the complex-type eigenenergies of the Fourier-grid Hamiltonian with the embedded optical potential can give results in an approximate description of the resonances but is not very reliable quantitatively. A brief introduction of the computer programs used in the present research and embedded into the Optimizer project is presented in the Appendix.

CRediT authorship contribution statement

Vladimir B. Sovkov: Writing – original draft, Software, Methodology, Investigation, Conceptualization. **Jizhou Wu:** Writing – review & editing, Investigation. **Jie Ma:** Writing – review & editing, Investigation. **Feng Xie:** Writing – review & editing, Investigation. **A.M. Lyyra:** Writing – review & editing, Investigation. **Ergin Ahmed:** Writing – review & editing, Investigation.

Declaration of competing interest

The authors declare that they have no known competing financial interests or personal relationships that could have appeared to influence the work reported in this paper.

Data availability

The data that support the findings of this study are openly available in the repository Source Forge at https://sourceforge.net/projects/optimizer-sovkov/, Ref. [2]. They include the open-source codes in Matlab of all the programs referred to and used here, their manuals, and examples enabling a reproduction of all the numerical results.

Acknowledgments

This work is supported by the National Natural Science Foundation of China (62020106014, 62175140), 111 project (D18001), the Shanxi

Appendix A. Padé approximants in the optimizer project

The Padé approximant [52] of a dependence $y(x)$ can be defined as:

$$y(x) = C + \frac{P_n(x)}{P_d(x)} \equiv$$
$$C + \frac{\sum_{k=0}^{N_n} a_k (x - x_0)^k}{\sum_{k=0}^{N_d} b_k (x - x_0)^k} \tag{6}$$

Equivalent forms parameterize the polynomials $P_n(x)$ and $P_d(x)$ via their nodes $z_k^{n/d}$ in place of the coefficients a_k and b_k:

$$P_{n/d} = C_{n/d} \prod_{k=1}^{N_{n/d}} (x - z_k^{n/d}). \tag{7}$$

For real-type functions, the nodes $z_k^{n/d}$ can either be real-type or pairs of mutually conjugated complex-type nodes. Our program supports both types of the parameterization.

A polynomial is a partial case of the Padé approximant with $P_d(x) = 1$, but in general, it is an approximation tool that has greater power. A relatively simple analytical form allows one to easily manage analytical properties such as poles, zeros, extrema, inflction points, asymptotes, *etc.*

Prospects of using the Padé approximants to describe potential energy curves of molecules have been discussed for several decades [53–65]. Nonetheless, their application in this field is still rather limited. One of the reasons is that, sometimes in the course of the optimization (fit) process, they can produce unexpected features, such as undesirable poles, bends, *etc.*, between the nodes of a computational grid, while at the nodes everything looks fine; we encountered such problems with first versions of our programs. Murrel et al. [58], based on their test computations, did not recommend using Padé approximants for this purpose. A recent review [79] presenting 50 most popular analytical representations of potential energy functions did not even include the Padé approximants in this list.

However, these difficulties are easily overcome within the mechanisms of the Optimizer project. At every step of the optimization process, the desirable properties (absence of poles, absence or existence of predefined number of extrema and inflection points in any predefined range, *etc.*) can be checked either analytically or numerically, in a case of their violation causing a break of the computation and an automatic reduce of the optimization step until the desired properties are fulfilled. In part, we successfully used this strategy in the present work.

The potential energy functions of molecules at large interatomic distances $R \equiv x$ are expected [66] to exhibit the inverse-power character:

$$U(R \sim \infty) \sim C + C_1/R^{N_1} + C_2/R^{N_2} + \cdots$$

with the leading powers depending on the state of a molecule (rather often, $N_1 = 3$, $N_2 = 6$, ...), while the so-called dispersion coefficients (C_1, C_2, ...) are either precomputed or estimated from experimental data. The Padé approximants can easily ensure a desirable asymptotic behavior.

Indeed, making the leading asymptotic term to be $\sim 1/R^{N_1}$ is achieved via making the power N_d of the polynomial $P_d(x)$ in Eq. (6) bigger than the power N_n of $P_n(x)$ by N_1, *i. e.*, $N_1 = N_d - N_n$, with $C_1 = a_{N_n}/b_{N_d}$. Then, assuming $x_0 = 0$ and substituting $q = 1/x$,

$$\frac{\sum_{k=0}^{N_n} a_k x^k}{\sum_{k=0}^{N_d} b_k x^k} - \frac{a_{N_n}}{b_{N_d}} \frac{1}{x^{N_d - N_n}} = q^{N_d - N_n} \times$$
$$\frac{\sum_{k=0}^{N_n-1} a_k q^{N_n - k} - (a_{N_n}/b_{N_d}) \sum_{k=0}^{N_d-1} b_k q^{N_d - k}}{\sum_{k=0}^{N_d} b_k q^{N_d - k}}.$$

Hence, for the next asymptotic term:

$$N_{next} = N_d - N_n + 1,$$
$$C_{N_{next}} = \frac{a_{N_n - 1} - (a_{N_n}/b_{N_d}) b_{N_d - 1}}{b_{N_d}}.$$

The latter relation enables setting this term to any desirable value (including the zero one) via fixing the approximant structure and equating a part of its coefficients to some definite values.

For example, in order to the leading asymptotic term to be $\sim 1/x^3$, the power of the polynomial in the denominator must be bigger than the power of the polynomial in the numerator by 3: $N_d = N_n + 3$. The easiest way to ensure the behavior of $\sim 1/x^6$ for the next asymptotic term is (with $x_0 = 0$) to equate to zero two penultimate coefficients a_k and three penultimate coefficients b_k. If $b_{N_d} = 1$, then the leading dispersion coefficient C_1 will be just equal to a_{N_n} and the next one C_2 will be equal to the last nonzero penultimate coefficients $a_{k'}$ (with $k' = N_n - 3$ in our example). It is easy to extend this reasoning to asymptotic terms of higher orders.

Our program can handle the following problems:

- Compute values y_i of the Padé function (6), (7) at a predefined grid $\{x_i\}$ using a predefined set of parameters.
- Compute values of the function and its derivatives of predefined orders at a set of some extra points.
- Impose constraints of the equality of the function itself and/or its derivatives of predefined orders at predefined points to predefined values via correction of a predefined set of parameters.
- Compute the local design matrix (Jacobi matrix) of the dependence

  $$y_i = f(\{a_k\}, \{b_k\}, x_0, C_{add}, C_{mul})$$

  or the equivalent dependence on the nodes $z_k^{n/d}$ in place of a_k, b_k, in accordance with the regulations of the package Optimizer [2].
- Compute the polynomial coefficients a_k, b_k Eq. (6) from the nodes $z_k^{n/d}$ Eq. (7) or vice versa.
- Compute coordinates and function values of the extrema and the inflection points.
- Estimate coefficients at $1/x^p$ (including positive and negative integer p) in the long-range asymptote $x \to \infty$.
- Support working with a composite function, when the formal variable x is a predefined function of a physical variable R.

A more comprehensive manual is accessible online [2], with the program codes and executable samples.

Appendix B. Split-operator method in the optimizer project

The Split-operator method [42–48] is a kind of the so-called pseudospectral methods. It is aimed at a simulation of the dynamics of a quantum system and, based on it, of a probability (intensity) distribution in a spectrum of a transition in such a system.

The quantum evolution operator at a short time interval δt can be approximated with:

$$\mathcal{T}(\delta t) = \exp\left\{-\frac{i}{\hbar} H \delta t\right\} = \exp\left\{-\frac{i}{\hbar} K \delta t - \frac{i}{\hbar} U \delta t\right\} \approx$$
$$\exp\left\{-\frac{i}{\hbar} K \delta t/2\right\} \exp\left\{-\frac{i}{\hbar} U \delta t\right\} \exp\left\{-\frac{i}{\hbar} K \delta t/2\right\} \approx \tag{8}$$
$$\exp\left\{-\frac{i}{\hbar} U \delta t/2\right\} \exp\left\{-\frac{i}{\hbar} K \delta t\right\} \exp\left\{-\frac{i}{\hbar} U \delta t/2\right\},$$

where H is the Hamiltonian, $K = -\frac{\hbar^2}{2m} \frac{\partial^2}{\partial R^2}$ is the operator of the system kinetic energy and $U(R)$ is the potential energy (generally, multichannel as in Eq. (1)). These forms are unitary, symmetrical and keep an important property of the time reversibility. Further on, we name these two approximations the KUK and UKU forms.

The operator $\exp\left\{-\frac{i}{\hbar} U \delta t\right\}$ is diagonal relative the coordinate R in the coordinate representation and relative the channel index in the adiabatic representation, *i.e.*, its action on a wavepacket is easily computed

(as just a multiplication) in the coordinate adiabatic representation. Analogously, the action of the operator $\exp\left\{-\frac{i}{\hbar}K\delta t\right\}$ is easily computed in the momentum diabatic representation. As is well known from Quantum Mechanics, the transform between the coordinate and momentum representations and *vice versa* is just the Fourier transform, while the transform between the adiabatic and diabatic representations is done with the transform matrices analogous to Eq. (4). This means that the evolution of a wavepacket $\psi(t = 0, R)$ in an entire time range can be computed as a sequence of its multiplication by one diagonal operator in one of these representation at a reasonably short time interval δt, transform to the other representation, multiplication by another diagonal operator, transform back to the first representation, and so on until the desired final time is achieved.

For a computing of the evolution of a bound state, no extra complications are needed. However, if a free (decaying) state is considered, some artificial features arise, which should be damped. Indeed, the spatial computational grid is anyway finite, so, when the modeled wavepacket arrives at its boundary, it is partially reflected from it and partially enters the grid from the opposite boundary (in the theory of the Fourier transform, it is called the aliasing effect), demonstrating nonphysical behavior. To overcome this drawback, absorbing boundary conditions or an imaginary-type "optical" potential [72] are usually embedded.

When an optical transition of a molecule from an initial state with the wavefunction $\varphi(R)$ into a (multichannel) system of final states is considered, the initial multichannel wavepacket $\psi(t = 0, R)$ is constructed via a multiplication of $\varphi(R)$ by a corresponding transition moment function $M_k(R)$ in every kth channel: $\psi_k(t = 0, R) = M_k(R)\varphi(R)$. Then the evolution $\psi(t, R)$ is calculated the way described above with the estimate at every time instant of a time autocorrelation function

$$S(t) = \langle\psi(t = 0, R)|\psi(t, R)\rangle$$

and the distribution of the transition probability (the spectrum of the transition) is estimated as the Fourier transform of the autocorrelator $S(t)$ (see also [46]).

We wrote and adapted to the Optimizer project several variants of the Split-operator programs. First, we realized both KUK and UKU schemes Eq. (8). Our test computations have shown that these two schemes possess approximately equivalent accuracy, however the KUK scheme is a little bit faster (see the manual [2] for an explanation why). Then, every program is written in both pure Matlab codes (vMatlab versions) and with blocks written in C and embedded with the help of the Matlab mex-mechanism (vMatlabC versions). The vMatlabC versions are several times faster than the vMatlab version but have a somewhat poorer functionality, that is not nevertheless important for the majority of prospective applications. The absorbing boundary conditions described in our recent work [72] are supported by all the versions.

A more detailed manual is available on the internet [2], along with the program codes and executable samples.

References

[1] Sovkov VB, Ma J. Matlab tool optimizer: Construction and optimization of multi-block mathematical models—application to spectroscopy experiments with ultracold gases of alkali metals. In: Dadvand A, Nagaraja K, Mirzazadeh M, editors. Proceedings of the 2016 international conference on applied mathematics, simulation and modelling. Advances in computer science research, volume 41, Beijing, China: Atlantis Press; 2016, p. 369–72. http://dx.doi.org/10.2991/amsm-16.2016.83, (No. 083).

[2] Sovkov VB. Optimizer: source codes and manuals & collection of applications. Online; 2019–2023, URL: https://sourceforge.net/projects/optimizer-sovkov/.

[3] Arndt PT, Sovkov VB, Ma J, Pan X, Beecher DS, Tsai JY, Livingston R, Marcune VM, Lyyra AM, Ahmed EH. Experimental study of the $3^3\Pi_g$ and $4^3\Sigma_g^+$ states of the rubidium dimer. Phys Rev A 2022;105:032823. http://dx.doi.org/10.1103/PhysRevA.105.032823.

[4] Onishchenko SS, Sovkov VB, Xie F, Li D, Lukashov SS, Baturo VV, Wu J, Ma J. Analysis of the hyperfine structure of the $1^3\Delta_g$, $2^3\Pi_g$, and $3^3\Sigma_g^+$ states of $^6Li^7Li$. J Quant Spectrosc Radiat Transfer 2021;270:107665. http://dx.doi.org/10.1016/j.jqsrt.2021.107665.

[5] Wang X, Liu W, Li Y, Wu J, Sovkov VB, Ma J, Onishchenko S, Li P, Fu Y, Li D, Fan Q, Xiao L, Jia S. Hyperfine structure of the NaCs $b^3\Pi_2$ state near the dissociation limit $3S_{1/2} + 6P_{3/2}$ observed with ultracold atomic photoassociation. Phys Chem Chem Phys 2020;22:3809–16. http://dx.doi.org/10.1039/C9CP05870B.

[6] Onishchenko SS, Sovkov VB, Xie F, Li D, Lukashov SS, Baturo VV, Wu J, Ma J, Li L. Analysis of the hyperfine structure of the Cs$_2$ $3^3\Sigma_g^+$ state. J Quant Spectrosc Radiat Transfer 2020;250:107037. http://dx.doi.org/10.1016/j.jqsrt.2020.107037.

[7] Arndt PT, Sovkov VB, Ma J, Pan X, Beecher DS, Tsai JY, Guan Y, Lyyra AM, Ahmed EH. Experimental study of the $6^1\Sigma_g^+$ state of the rubidium dimer. Phys Rev 2019;99:052511. http://dx.doi.org/10.1103/PhysRevA.99.052511.

[8] Feng G, Xie F, Sovkov VB, Ma J, Xiao L, Jia S. Nonadiabatic coupling of molecular states in presence of unobserved perturbers: Modeling and analysis. J Phys Soc Japan 2018;87:024303. http://dx.doi.org/10.7566/JPSJ.87.024303.

[9] Arndt PT, Sovkov VB, Ma J, Pan X, Beecher DS, Tsai JY, Guan Y, Lyyra AM, Ahmed EH. The Rb$_2$ $3^1\Pi_g$ state: Observation and analysis. J Chem Phys 2018;149:224303. http://dx.doi.org/10.1063/1.5058282.

[10] Sovkov VB, Xie F, Li D, Lukashov SS, Baturo VV, Ma J, Li L. Renewed analysis of the hyperfine structure of the Na$_2$ $1^3\Delta_g$ state. AIP Adv 2018;8:125322. http://dx.doi.org/10.1063/1.5055675.

[11] Sovkov VB, Xie F, Lyyra AM, Ahmed EH, Ma J, Jia S. Re-examination of the Cs$_2$ ground singlet $X^1\Sigma_g^+$ and triplet $a^3\Sigma_u^+$ states. J Chem Phys 2017;147:104301. http://dx.doi.org/10.1063/1.5001481, see erratum in [12].

[12] Sovkov VB, Xie F, Lyyra AM, Ahmed EH, Ma J, Jia S. Erratum: Re-examination of the Cs$_2$ ground singlet $X^1\Sigma_g^+$ and triplet $a^3\Sigma_u^+$ states [J. Chem. Phys. 147 (2017) 104301]. J Chem Phys 2018;149:239901. http://dx.doi.org/10.1063/1.5083024, erratum to [11].

[13] Liu W, Wu J, Ma J, Li P, Sovkov VB, Xiao L, Jia S. Observation and analysis of the hyperfine structure of near-dissociation levels of the NaCs $c^3\Sigma^+$ state below the dissociation limit $3S_{1/2} + 6P_{3/2}$. Phys Rev A 2016;94:032518. http://dx.doi.org/10.1103/PhysRevA.94.032518.

[14] Yang J, Guan Y, Zhao W, Zhou Z, Han X, Ma J, Sovkov VB, Ivanov VS, Ahmed EH, Lyyra AM, Dai X. Observations and analysis with the spline–based Rydberg–Klein–Rees approach for the $3^1\Sigma_g^+$ state of Rb$_2$. J Chem Phys 2016;144:024308. http://dx.doi.org/10.1063/1.4939524.

[15] Liu W, Xu R, Wu J, Yang J, Lukashov SS, Sovkov VB, Dai X, Ma J, Xiao L, Jia S. Observation and deperturbation of near–dissociation ro–vibrational structure of the Cs$_2$ state 0_u^+ ($A^1\Sigma_u^+ \sim b^3\Pi_{0+u}$) at the asymptote $6S_{1/2} + 6P_{1/2}$. J Chem Phys 2015;143:124307. http://dx.doi.org/10.1063/1.4931646.

[16] Ma J, Liu W, Yang J, Wu J, Sun W, Ivanov VS, Skublov AS, Sovkov VB, Dai X, Jia S. New observation and combined analysis of the Cs$_2$ 0_u^-, 0_u^+ and 1_g states at the asymptotes $6S_{1/2} + 6P_{1/2}$ and $6S_{1/2} + 6P_{3/2}$. J Chem Phys 2014;141:244310. http://dx.doi.org/10.1063/1.4904265.

[17] Sovkov VB, Li D, Ivanov VS, Skublov AS, Xie F, Li L, Magnier S. Two–photon excitations of the Cs$_2$ $3^3\Sigma_g^+$ state: Assignment and analysis with the deformed *ab initio* potential. Chem Phys Lett 2013;557:66–70. http://dx.doi.org/10.1016/j.cplett.2012.12.030.

[18] Guan Y, Han X, Yang J, Zhou Z, Dai X, Ahmed EH, Lyyra AM, Magnier S, Ivanov VS, Skublov AS, Sovkov VB. Updated potential energy function of the Rb$_2$ $a^3\Sigma_u^+$ state in the attractive and repulsive regions determined from its joint analysis with the $2^3\Pi_{0g}$ state. J Chem Phys 2013;139:144303. http://dx.doi.org/10.1063/1.4823496.

[19] Xie F, Li L, Li D, Sovkov VB, Minaev KV, Ivanov VS, Lyyra AM, Magnier S. Joint analysis of the Cs$_2$ $a^3\Sigma_u^+$ and 1_g ($3^3\Pi_{1g}$) states. J Chem Phys 2011;135:024303. http://dx.doi.org/10.1063/1.3606397.

[20] Marquardt DW. An algorithm for least–squares estimation of nonlinear parameters. J Soc Ind Appl Math 1963;11:431–41. http://dx.doi.org/10.1137/0111030.

[21] Levenberg K. A method for the solution of certain non-linear problems in least squares. Quart Appl Math 1944;2:164–8, URL: http://www.jstor.org/stable/43633451.

[22] Golub GH, van Loan CF. Matrix computations. third ed.. Baltimore and London: The John Hopkins University Press; 1996, URL: https://jhupbooks.press.jhu.edu/content/matrix-computations.

[23] MathWorks. Matlab online documentation. online; 2019, URL: https://www.mathworks.com/help/matlab/index.html.

[24] Eaton JW, et al. GNU octave: scientific programming language (online). online; 2019, URL: https://www.gnu.org/software/octave/.

[25] Liu Y, Li J, Gao H, Li L, Field RW, Lyyra AM. Predissociation of the Na$_2$ $3^3\Pi_g$ and other triplet states. J Chem Phys 1998;108:2269–76. http://dx.doi.org/10.1063/1.475611.

[26] Li L, Field RW. Direct observation of high–lying $^3\Pi_g$ states of the Na$_2$ molecule by optical–optical double resonance. J Phys Chem 1983;87:3020–2. http://dx.doi.org/10.1021/j100239a011.

[27] Li L, Rice SF, Field RW. The Na$_2$ $a^3\Sigma_u^+$ state. Rotationally resolved OODR $^3\Pi_g \rightarrow a^3\Sigma_u^+$ fluorescence spectroscopy. J Chem Phys 1985;82:1178–82. http://dx.doi.org/10.1063/1.448490.

[28] Li L, Field RW. CW optical–optical double resonance studies of the $2^3\Pi_g$, $3^3\Pi_g$, $4^3\Pi_g$, and $1^3\Delta_g$ Rydberg states of Na_2. J Mol Spect 1986;117:245–82.

[29] Whang T-J, Stwalley WC, Li L, Lyyra AM. Perturbation–facillitated all–optical spectroscopy of the Na_2 $b^3\Pi_u$ state. J Chem Phys 1992;97:7211–8.

[30] Whang T-J, Tsai C-C, Stwalley WC, Lyyra AM, Li L. Spectroscopic study of the Na_2 $2^3\Sigma_g^+$ state by cw perturbation–facilitated optical–optical double–resonance spectroscopy. J Mol Spectrosc 1993;160:411–21.

[31] Li L, Yiannopoulou A, Urbanski K, Lyyra AM, Ji B, Stwalley WC, An T. Hyperfine structures of the $^7Li_2$ $b^3\Pi_u$, $2^3\Pi_g$, and $3^3\Pi_g$ states: Continuous wave perturbation facilitated optical–optical double resonance spectroscopy. J Chem Phys 1996;105:6192–9, ERRATA: [32].

[32] Li L, Yiannopoulou A, Urbanski K, Lyyra AM, Ji B, Stwalley WC, An T. Erratum: Hyperfine structures of the $^7Li_2$ $b^3\Pi_u$, $2^3\Pi_g$, and $3^3\Pi_g$ states: Continuous wave perturbation facilitated optical–optical double resonance spectroscopy [J. Chem. Phys. 105 (1996) 6192]. J Chem Phys 1997;106:8626, ERRATA to: [31].

[33] Li J, Liu Y, Chen H, Xiang J, Chen D, Wu G, Li L. Predissociation of the Na_2 $4^3\Sigma_g^+$ state. J Chem Phys 1998;108:7707–12. http://dx.doi.org/10.1063/1.476206.

[34] Li L, Lyyra AM. Triplet states of Li_2 and Na_2: Perturbation facilitated optical–optical double resonance spectroscopy. Spectrochim Acta 1999;55:2147–78. http://dx.doi.org/10.1016/S1386-1425(99)00091-8.

[35] Li L, Lazoudis A, Yi P, Liu Y, Huennekens J, Field RW, Lyyra AM. Hyperfine structure of the $1^3\Delta_g$, $2^3\Pi_g$, and $3^3\Sigma_g^+$ states of $^6Li^7Li$. J Chem Phys 2002;116:10704–12. http://dx.doi.org/10.1063/1.1478692.

[36] Xie F, Li D, Li L, Field RW, Magnier S. Infrared–infrared double resonance spectroscopy of $^{39}K_2$: The $1^3\Delta_g$ state. Chem Phys Lett 2006;431:267–71. http://dx.doi.org/10.1016/j.cplett.2006.10.002.

[37] Magnier S, Millié P, Dulieu O, Massnou-Seeuws F. Potential curves for the ground and excited states of the Na_2 molecule up to the $(3s + 5p)$ dissociation limit: Results of two different effective potential calculations. J Chem Phys 1993;98:7113–25. http://dx.doi.org/10.1063/1.464755.

[38] Taylor JR. Scattering theory: the quantum theory on nonrelativistic collisions. New York–London–Sydney–Toronto: John Wiley & Sons; 1972, URL: https://store.doverpublications.com/0486450139.html.

[39] Katô H, Baba M. Dynamics of excited molecules: Predissociation. Chem Rev 1995;95:2311–49. http://dx.doi.org/10.1021/cr00039a003.

[40] Brzozowski J, Bunker P, Elander N, Erman P. Predissociation effects in the A, B and C states of CH and the interstellar formation rate of CH via inverse predissociation. Astrophys J 1976;207:414–24. http://dx.doi.org/10.1086/154509.

[41] Brzozowski J, Elander N, Erman P, Lyyra M. On the interstellar abundance of CH^+ radical. Astrophys J 1974;193:741–5. http://dx.doi.org/10.1086/153213.

[42] Feit JA, Fleck Jr MD, Steiger A. Solution of the Schrödinger equation by a spectral method. J Comput Phys 1982;47:412–33. http://dx.doi.org/10.1016/0021-9991(82)90091-2.

[43] Feit MD, Fleck Jr JA. Solution of the Schrödinger equation by a spectral method II: Vibrational energy levels of triatomic molecules. J Chem Phys 1983;78:301–8. http://dx.doi.org/10.1063/1.444501.

[44] Heather R, Metiu H. An efficient procedure for calculating the evolution of the wave function by fast Fourier transform methods for systems with spatially extended wave function and localized potential. J Chem Phys 1987;86:5009–17. http://dx.doi.org/10.1063/1.452672.

[45] Alvarellos J, Metiu H. The evolution of the wave function in a curve crossing problem computed by a fast Fourier transform method. J Chem Phys 1988;88:4957–66. http://dx.doi.org/10.1063/1.454707.

[46] Engel V. The calculation of autocorrelation functions for spectroscopy. Chem Phys Lett 1992;189:76–8. http://dx.doi.org/10.1016/0009-2614(92)85155-4.

[47] Serov VN, Sovkov VB, Ivanov VS, Atabek O. Split operator method for the nonadiabatic $(J = 0)$ bound states and $(A \leftarrow X)$ absorption spectrum of NO_2. J Chem Phys 2001;115:6450–8. http://dx.doi.org/10.1063/1.1396854.

[48] Zhang C-X, Niu Y-Q, Meng Q-T. Time-dependent approach to the double-channel dissociation of the NaCs molecule induced by pulsed lasers. Chin Phys B 2014;23:103301. http://dx.doi.org/10.1088/1674-1056/23/10/103301.

[49] Ivanov VS, Serov VN, Sovkov VB. Simulation of predissociation spectra with the multichannel split operator technique. In: Bludský O, Pracna P, Špirko V, Urban Š, editors. Book of abstracts: the 16-th international conference on high resolution molecular spectroscopy. Prague, Czech Republic: J. Heyrovský Institute of Physical Chemistry of Academy of Sciences of the Czech Republic; 2000, p. 48, (D10). URL: http://www.chem.uni-wuppertal.de/conference.

[50] Narevicius E, Moiseyev N, Sadeghpour HR, Cederbaum LS. Extremely narrow peaks in predissociation of sodium dimer due to rovibronic coupling. J Chem Phys 2004;121:3527–32. http://dx.doi.org/10.1063/1.1773171.

[51] Moiseyev N. Quantum theory of resonances: Calculating energies, widths and cross–sections by complex scaling. Phys Rep 1997;302:211–93.

[52] Baker GA, Graves-Morris P. Padè approximants, In: Encyclopedia of mathematics and its applications, second ed.. volume 59, Cambridge, UK: Cambridge University Press; 1996, http://dx.doi.org/10.1017/CBO9780511530074.

[53] Jordan KD, Kinsey JL, Silbey R. Use of Pade approximants in the construction of diabatic potential energy curves for ionic molecules. J Chem Phys 1974;61:911–7. http://dx.doi.org/10.1063/1.1682034.

[54] Jordan KD. Padè approximants: An alternative analytic representation of the potential curves for diatomic molecules. J Mol Spectrosc 1975;56:329–31. http://dx.doi.org/10.1016/0022-2852(75)90243-X.

[55] Engelke R. Diatomic molecule vibrational potentials: Accuracy of representations. J Chem Phys 1978;68:3514–21. http://dx.doi.org/10.1063/1.436261.

[56] Engelke R. Diatomic-molecule vibrational potentials. II. New representations. J Chem Phys 1979;70:3745–57. http://dx.doi.org/10.1063/1.437980.

[57] Pardo A, Camacho JJ, Poyato JML. The Padè-approximant method and its applications in the construction of potential-energy curves for the lithium hydride molecule. Chem Phys Lett 1986;131:490–5. http://dx.doi.org/10.1016/0009-2614(86)80570-X.

[58] Murrell JN, Varandas AJC, Brandão J. The rational fraction representation of diatomic potentials. Theor Chim Acta 1987;71:459–65. http://dx.doi.org/10.1007/BF00530243.

[59] Golovko V, Mikhailenko S, Tyuterev V. Application of the Pade-form Hamiltonians for processing of vibration–rotation spectra of diatomic and triatomic molecules. J Mol Struct 1990;218:291–6. http://dx.doi.org/10.1016/0022-2860(90)80282-O.

[60] Golovko V, Mikhailenko SN, Tyuterev VIG. Combined application of the Padè technique and the RKR method for the extrapolation of the function of potential energy of diatomic molecules. Opt Spectrosc 1996;81:677–9, URL: https://elibrary.ru/item.asp?id=13234428.

[61] Molski M, Konarski J. A generalized expansion of the potential energy of diatomic molecules. Int J Quantum Chem 2002;90:183–7. http://dx.doi.org/10.1002/qua.978.

[62] Castro E, Martín P, Paz J. Precise spectra for the H_2 molecule by a new approximate technique. Phys Lett, Sect A 2007;364:135–9. http://dx.doi.org/10.1016/j.physleta.2006.11.081.

[63] Voitsekhovskaya O, Kalashnikov A, Cherepanov V. Application of the Padé approximations to calculation of rotational energies of a triatomic linear molecule. Russian Phys J 2006;49:960–3. http://dx.doi.org/10.1007/s11182-006-0209-3.

[64] Landau A, Ben-Asher A, Gokhberg K, Cederbaum L, Moiseyev N. Ab initio complex potential energy curves of the He^* $(1s2p^1P)$-Li dimer. J Chem Phys 2020;152:0008337. http://dx.doi.org/10.1063/5.0008337.

[65] Babenko V, Petrov N. On the quantum anharmonic oscillator and Padé approximations. Nucl Phys Atom Energy 2021;22:127–42. http://dx.doi.org/10.15407/jnpae2021.02.127.

[66] Lefebvre-Brion H, Field RW. The spectra and dynamics of diatomic molecules, elsevier. Amsterdam–Boston–Heidelberg–New York–Oxford-Paris–San Diego–San Francisco–Singapore–Sydney–Tokyo: Academic Press; 2004, URL: http://www.sciencedirect.com/science/book/9780124414556.

[67] Landau LD, Lifshitz EM. Quantum mechanics. non-relativistic theory. Oxford–New York–Toronto–Sydney–Paris–Frankfurt: Pergamon; 1977, http://dx.doi.org/10.1016/C2013-0-02793-4.

[68] N. I. of standards, NIST online databases. 2023, URL: https://www.nist.gov/pml/atomic-spectra-database.

[69] Qi P, Lazarov G, Lyyra AM, Liu Y, Cui C, Li L, Jeung G-H. The Na_2 $2^3\Pi_g$ state: New observations and hyperfine structure. J Chem Phys 2006;124:184304. http://dx.doi.org/10.1063/1.2190217.

[70] Blatt JM. Practical points concerning the solution of the Schrödinger equation. J Comput Phys 1967;1:382–96. http://dx.doi.org/10.1016/0021-9991(67)90046-0.

[71] Qi P, Bai J, Ahmed E, Lyyra AM, Kotochigova S, Ross AJ, Effantin C, Zalicki P, Vigué J, Chawla G, Field RW, Whang T-J, Stwalley WC, Knöckel H, Tiemann E, Shang J, Li L, Bergeman T. New spectroscopic data, spin–orbit functions, and global analysis of data on the $A^1\Sigma_u^+$ and $b^3\Pi_u$ states of Na_2. J Chem Phys 2007;127:044301. http://dx.doi.org/10.1063/1.2747595.

[72] Sovkov VB, Wu J, Ma J. Cosine-type absorbing optical potential for the modeling of quantum dynamics with the Fourier grid and Optimizer packages. Opt Spectrosc 2022;130:513–23. http://dx.doi.org/10.21883/EOS.2022.05.54434.7-22.

[73] Martson CC, Balint-Kurti GG. The Fourier grid Hamiltonian method for bound state eigenvalues and eigenfunctions. J Chem Phys 1989;91:3571–6. http://dx.doi.org/10.1063/1.456888.

[74] Kokoouline V, Dulieu O, Kosloff R, Masnou-Seeuws F. Mapped Fourier methods for long–range molecules: Application to perturbations in the Rb_2 0_u^+ photoassociation spectrum. J Chem Phys 1999;110:9865–76. http://dx.doi.org/10.1063/1.478860.

[75] Lemoine D. Optimized grid representations in curvilinear coordinates: The mapped sine Fourier method. Chem Phys Lett 2000;320:492–8. http://dx.doi.org/10.1016/S0009-2614(00)00269-4.

[76] Willner K, Dulieu O, Masnou-Seeuws F. Mapped grid methods for long–range molecules and cold collisions. J Chem Phys 2004;120:548–61. http://dx.doi.org/10.1063/1.1630031.

[77] Li L, Liu Y, Lyyra AM. Rydberg and doubly excited states of Na_2 and Li_2. J Chin Chem Soc 2001;48:291–9. http://dx.doi.org/10.1002/jccs.200100046.

[78] Xie X, Field RW, Li L, Marjatta Lyyra A, Bahns JT, Stwalley WC. Absolute vibrational numbering and molecular constants of the Na_2 $2^3\Pi_g$ state. J Mol Spectrosc 1989;134:119–28. http://dx.doi.org/10.1016/0022-2852(89)90134-3.

[79] Araújo JP, Ballester MY. A comparative review of 50 analytical representation of potential energy interaction for diatomic systems: 100 years of history. Int J Quantum Chem 2021;121:e26808. http://dx.doi.org/10.1002/qua.26808.